MITIGATING DISTORTION DURING SINTERING OF BINDER JET PRINTED CERAMICS

Lynnora O. Grant[1], Magdi B. Alameen[2], J. Reid Carazzone[1], C. Fred Higgs III[3], Zachary C. Cordero[1]

[1] Rice University, Department of Materials Science and NanoEngineering
[2] University of Houston, Department of Chemical Engineering
[3] Rice University, Department of Mechanical Engineering

ABSTRACT

Sintering increases the strength of binder jet 3D printed green bodies through densification, but with the potential cost of distortion due to creep. In this work, we determine how a reactive binder affects such distortion during sintering of titanium dioxide green bodies. The binder decomposes to form nanocrystalline interparticle necks during the early stages of the sintering process. We first characterize the decomposition of the reactive binder through thermogravimetry, differential scanning calorimetry, and x-ray diffraction. Next, we elucidate the effect of this precursor on the shrinkage of cylindrical parts using dilatometry experiments, and observe the deflection of sintering beams using *in situ* imaging. These experiments show that the precursor dramatically suppresses creep during sintering, demonstrating a potential solution for increasing the dimensional accuracy of the binder jet 3D printing process.

1. INTRODUCTION

Binder jet three-dimensional (3D) printing is a low-cost, high-throughput additive manufacturing technique in which a part is built layer-by-layer by selectively joining powder particles with an organic binder. Binder jet printing has been used to manufacture metallic [1] and ceramic [2] net-shaped green bodies. These as-printed parts are often friable and must be densified through post-processing to create strong engineering components. A common approach for densifying monolithic parts is pressureless sintering, which involves exposing the parts to high temperatures to join particles and reduce porosity. Ideally, the green part should shrink uniformly during sintering; however, various factors can give rise to shear stresses that lead to non-uniform changes in shape (here referred to as distortion) [3]. In this work, the problem of distortion due to gravitational body forces is investigated.

The extent of distortion during sintering of porous crystalline materials is a function of material properties (e.g., surface energy, diffusivity, etc.), microstructural variables (e.g., particle shape, size, interparticle neck radius, relative density), and process parameters (e.g., sintering temperature and applied pressure) [4]. Crane et al. explored mitigating creep in binder jet printed steel beams by increasing the radii of interparticle necks in the powder aggregate. They printed cantilevered beams from 410 SS, then infiltrated the beams with an organic solvent suspension of iron nanoparticles [5]. During heat treatment, these iron nanoparticles sintered at low temperatures and increased the size of the necks between the 410 SS particles, increasing the effective viscosity of the part and therefore its resistance to creep.

An alternative approach to enhancing the interparticle bonds during sintering is to use reactive binders, which can be deposited as a liquid via the printhead, then reacted after the printing step to form solid interparticle bonds [6–8]. The advantage of this approach compared to using a binder that contains nanoparticles is that it eliminates problems with nanoparticles agglomerating and potentially clogging the printhead during binder deposition. This reactive binder approach was first demonstrated by Sachs and coworkers, who applied silver nitrate metal salts to stainless steel powder to strengthen the green body [9]. More recently, Bai et al. used an organometallic ink with copper (II) formate as the nanoparticle precursor. This reactive binder was deposited on a copper powder bed and cured with an overhead heater. Copper nanoparticles precipitated out of the binder during the firing process in a controlled-atmosphere oven, forming nanoparticle bridges at the particle contacts [10].

In the present work, we describe a method to mitigate distortion in a binder jet 3D printed ceramic system using a reactive liquid precursor. The metal oxide precursor solution is decomposed after printing to increase the interparticle neck size. We characterize the decomposition behavior of the reactive precursor and its interaction with green bodies, then we evaluate its effect on mitigating distortion during sintering through thermomechanical and *in situ* monitoring experiments.

2. STRUCTURAL EVOLUTION OF THE REACTIVE BINDER

In this work, an aqueous titanium (IV) bis (ammonium lactato) dihydroxide (TALH) 50 wt% solution from Sigma Aldrich (catalog number 388165) was applied to binder jet printed TiO_2 parts. TALH is a water soluble chelate material that has been used in the field of photovoltaics and, more recently, direct write 3D printing methods [11,12]. Aqueous TALH solutions have been decomposed to form titanium dioxide (TiO_2) nanoparticles through hydrothermal reactions [13], chelate destabilization reactions using acidic solutions [14], and photodecomposition reactions [15].

We investigated the decomposition of the TALH solution using thermogravimetric analysis (TGA), differential scanning calorimetry (DSC), and x-ray diffraction (XRD). **Figure 1a** is a TGA

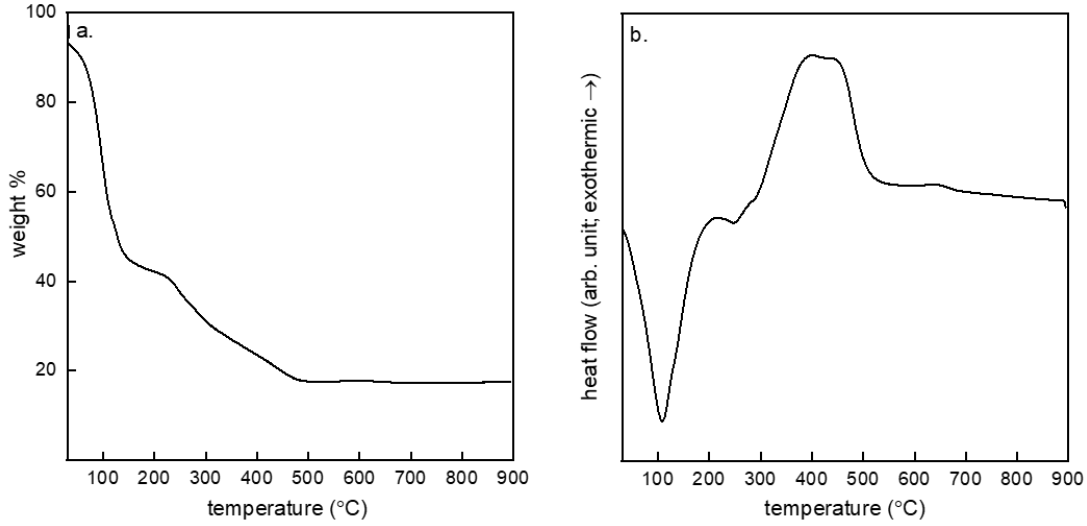

Figure 1. (a) TGA weight loss curve and (b) DSC thermogram during TALH solution thermal decomposition.

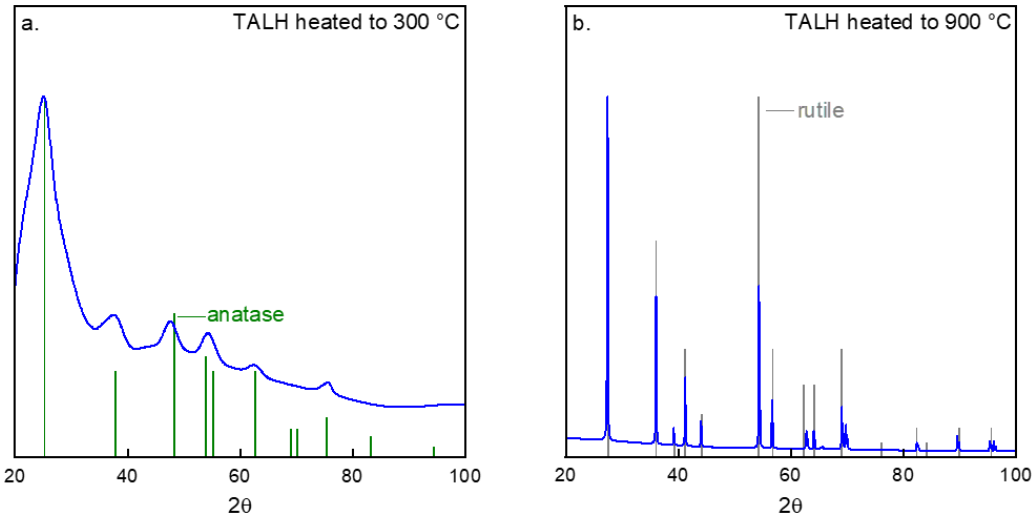

Figure 2. XRD patterns of products from TALH solution heated to (a) 300 °C and (b) 900 °C.

weight loss curve showing the change in weight of the TALH solution as a function of temperature while heating at a rate of 20 °C/min. There is a 50% reduction in mass around 100 °C, corresponding to water evaporation. A second period of mass loss occurs in the 250 to 500 °C temperature range, corresponding to decomposition of organic compounds [13]. At temperatures greater than 500 °C, the weight percent stabilizes around 17%, indicating the amount of TiO_2 obtained through decomposition. **Figure 1b** is a DSC thermogram that was collected during the TGA experiment. There is an endothermic peak around 100 °C due to water evaporation and an exothermic peak in the 250 to 500 °C range indicative of organic decomposition.

Figure 2 shows results from interrupted XRD measurements of the TALH solution after it had been heated to 300 °C and 900 °C at a rate of 6 °C/min and held for five minutes. A phase transformation from anatase to rutile was observed during heating. Additional XRD measurements revealed that this transition occurred in the range of 500 to 900 °C with both phases present at 700 °C. The decrease in the background noise from **Figure 2a** to **Figure 2b** denotes the removal of chemical impurities such as residual organic compounds. This observation is supported by the literature: at temperatures above 500 °C, the TALH decomposition reaction changes to yield gaseous ammonia, water, and carbon dioxide; these chemical impurities are thus removed from the system, leaving behind a TiO_2 residue [16]. A third observation from the XRD plots is the sharpening of the diffraction peaks from **Figure 2a** to **Figure 2b**, which corresponds to grain coarsening**.** In hydrothermal reactions reported in the literature, decomposition of the TALH solution begins at temperatures as low as 120 °C, forming anatase nanoparticles with a diameter of 3 nm [13]. When our sample was heated to 900 °C, coarser grains on the order

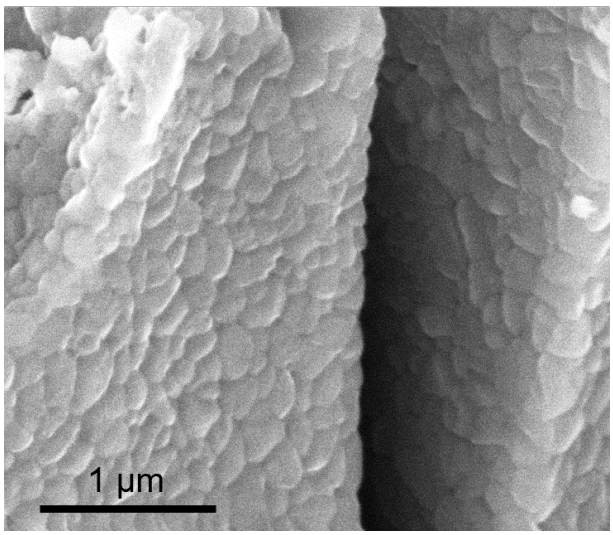

Figure 3. SEM micrograph of nanocrystalline TiO_2 formed by heating TALH to 900 °C for 5 minutes.

of 100 nm were present. This grain structure is evident in **Figure 3**, an SEM micrograph of the TiO2 produced by heating the TALH solution to 900 °C for five minutes.

By isolating the TALH solution and investigating its thermal behavior, it can be concluded that at sintering temperatures above 900 °C, rigid structures of rutile TiO_2 with a grain size on the order of 100 nm will be present in the system.

3. REACTIVE BINDER EVOLUTION IN 3D PRINTED GREEN BODIES

Green bodies were printed using a polydisperse rutile TiO_2 powder with a jagged particle shape and a mesh size of -230 (Saint-Gobain). The powder is 99% TiO_2 with 0.12% Al_2O_3 and trace amounts of other oxides. The parts were printed with an aqueous binder (ExOne, item number 7100037CL) with a saturation level of 90% and a 100 μm layer thickness. The microstructure of a printed and cured green body is shown by an SEM micrograph in **Figure 4a**. The solid material which forms a bond between the TiO2 particles is produced by heating the aqueous binder solution. Through TGA of a green body (ramp to 900 °C at 20 °C/min), we determined that the binder burnout process begins at 300 °C and finishes around 600 °C.

For select green bodies, TALH solution was directly applied to the samples via pipetting. The amount of TALH applied was equal to the theoretical volume of the pores in the green body, as determined by the mass-volume method. The green body with TALH was then heated to precipitate the TiO_2 nanoparticles. **Figure 4b** shows a TALH infiltrated sample that was heated to 700 °C for five minutes. TiO_2 derived from the decomposition of the TALH is evident as smaller particles covering most of the surface of the powder, revealing that at higher temperatures, after the binder has burned out, the precipitated TiO_2 nanoparticles can serve as a binding agent that strengthens the green printed parts. **Figure 4b** further shows that the TiO_2 coating partially fills the pores between particles, indicating a mechanism for shrinkage mitigation. These observations suggest that the TiO_2 nanostructures can serve as a secondary binding agent that strengthens the printed parts during and following binder burnout.

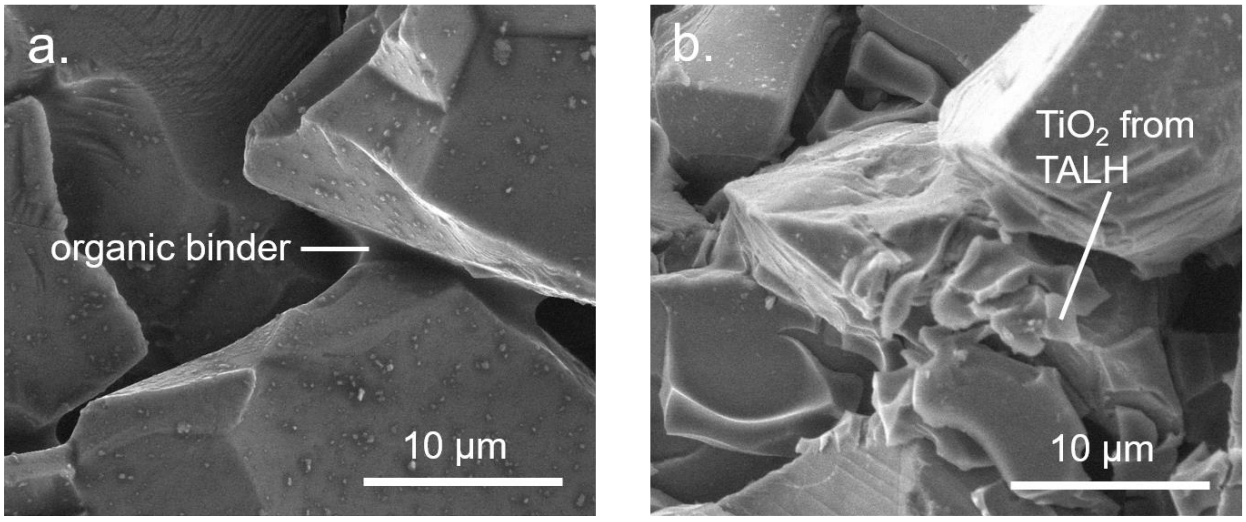

Figure 4. SEM micrographs of (a) green body with the aqueous binder cured by heating to 183 °C for 4 hours and (b) a TALH-infiltrated brown body that had been heated to 700 °C. In (b), note the flaky TiO_2 nanostructures produced from the thermal decomposition of TALH.

4. SINTERING EXPERIMENTS

4.1 Dilatometry experiments

Binder jet 3D printed cylindrical samples, 6.5 mm tall and 6.5 mm wide, were sintered under a uniaxial pressure in a NETZSCH thermomechanical analysis system (TMA). This TMA system is capable of measuring changes in sample height throughout the sintering process. For select cylinders, the applied TALH solution was decomposed by heating to 300 °C prior to sintering. The cylinders were sintered by heating to 1420 °C at a rate of 6 °C/min, then holding at 1420 °C (a homologous temperature of 0.8) for ten hours. The pre-specified uniaxial pressures of 0.3 and 3 kPa were applied continuously during sintering. A thin layer of soda-lime glass powder was applied between the alumina pushrod and the sample to prevent frictional adhesion.

Figure 5 shows engineering strain measurements as a function of temperature during the TMA experiments. These measurements were collected for four samples: TALH-treated samples under pressures of 0.3 kPa and 3 kPa, and untreated samples under the same pressures. When the temperature reached 500 °C, there was an abrupt increase in the shrinkage rate of the samples without TALH, presumably due to particle rearrangement during binder burnout. This behavior was not observed in the TALH-treated samples, suggesting that TiO_2 from decomposed TALH adds strength to the brown body (i.e., after binder burnout process). When the applied pressure was increased from 0.3 to 3 kPa, the compressive strain increased significantly in the untreated sample during the final stages of sintering. Thus, the untreated samples have a higher stress sensitivity: creep and densification occur faster in the untreated samples than in those treated with TALH. This difference in stress dependence reveals that the TiO_2 nanoparticles derived from the TALH have increased the effective viscosity of the cylinders.

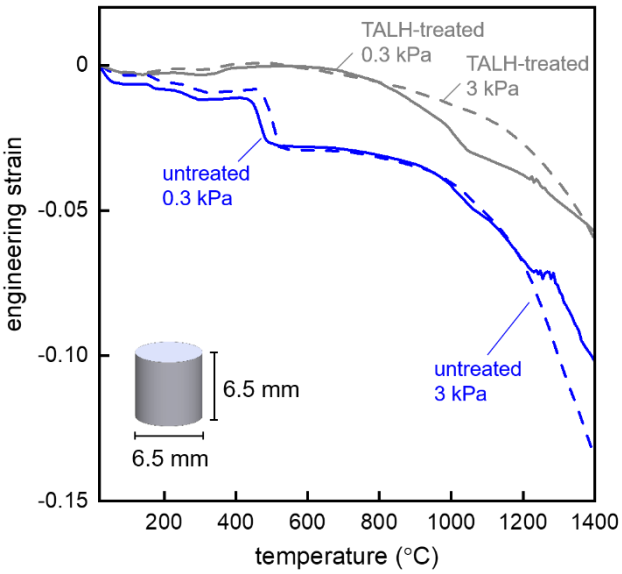

Figure 5. TMA results showing engineering strain for treated and untreated cylinders sintered under a uniaxial pressure. Cylinder dimensions are shown.

TALH treatment also had the effect of increasing the relative density of the samples. The initial average relative density for all the samples was around 39%. TALH-treated samples, after heating to 300 °C, had an average relative density of 48%. After sintering, the average relative density of the TALH-treated samples increased to 55%, whereas the untreated samples had a final relative density of 48%.

4.2 *In situ* monitoring of cantilevered beams during sintering

In a second set of experiments, *in situ* monitoring was used to directly observe the distortion behavior of binder jet printed cantilevered beams during sintering. To achieve a uniform densification rate that is independent of position, the beams were designed so that the sintering stress was greater than the maximum hydrostatic stress. The sintering stress was approximated by dividing the surface energy by the average particle size while the hydrostatic stress was calculated using elementary beam bending theory. The overhang of the symmetric beam was designed with a length of 10 mm, a height of 2.5 mm, and a width of 6 mm. A pre-sintering heat treatment was used to increase the handling strength of the specimens. During this step, beams were heated to 1100 °C (homologous temperature of 0.65) for one hour in a supported position to initiate neck growth. After the pre-sintering step, select beams were treated with TALH which was then decomposed by heating to 300 °C. Specimens were placed in a tube furnace, heated to the sintering temperature of 1420 °C over the course of 11 hours, then held at 1420 °C for 10 hours.

The beam specimens were monitored using a 22.3 megapixel Cannon SLR camera equipped with a 200 mm lens and 2x extender. Photographs were taken at five second intervals. **Figure 6a** shows three optical images of an untreated beam specimen, each at a different stage in the sintering process. In the first image, taken 7 hours into the sintering process, no deflection is observed. In the second and third images, taken after 10 and 21 hours respectively, deflection due to creep can be observed. A majority of the creep-induced deflection occurs above 1180 °C (homologous temperature of 0.68). **Figure 6b** shows similar optical images for a TALH-treated sample. Deflection in the TALH-treated beam is not visible in the image taken 10 hours into the experiment and the deflection visible in the image taken at 21 hours is significantly less than that in the untreated beam. The images reveal that the TALH treatment mitigated gravity-induced creep during sintering. The total deflection of the beams after sintering was measured through image analysis: the final deflection of the untreated beam was 4 mm whereas the deflection of the TALH-treated beam was 1 mm, a 75% reduction of distortion.

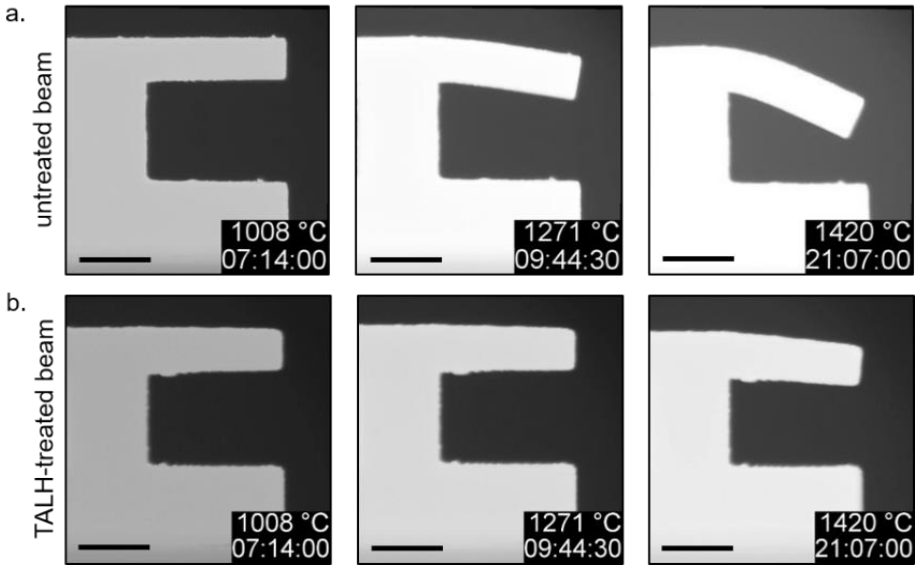

Figure 6. *In situ* images of (a) untreated and (b) TALH-treated cantilevered beams during sintering. Scale bars are 5 mm. Set temperature and time is shown.

5. CONCLUSION

We have presented a method for mitigating distortion during sintering of binder jet printed ceramic parts, using as a model system TiO_2 powder and the reactive liquid precursor, TALH. Through characterization using TGA, DSC, XRD, and SEM, the product of heating TALH to temperatures exceeding 900 °C was determined to be rutile TiO_2 with a grain size on the order of 100 nm. The reactive binder provides structural support in the brown body. This capability is useful when sintering ceramics, which generally require higher sintering temperatures than metallic engineering alloys and are therefore more susceptible to failure immediately after binder burnout.

Infiltration of porous cylindrical specimens with TALH led to lower uniaxial strains during sintering as measured by TMA. A dramatic decrease in deflection of TALH-treated cantilever beams was observed during sintering by means of *in situ* monitoring. The mechanism for this mitigation as revealed by SEM is the nanoparticle structure which results from the decomposition of TALH, coating the printed powder and filling the interparticle pores. Due to the lower sintering temperatures of nanoscale particles, such a coating has the potential to form a rigid, reinforcing structure early in the sintering cycle, thus strengthening the sintering body, increasing its viscosity, and enhancing its resistance to creep.

ACKNOWLEDGEMENTS

The project was funded using NSF grant number DGE# 1450681. The presenter also is grateful to have received a NSF application waiver for the conference. The authors would like to thank The ExOne Company for guidance during the early stages of the project. The authors would also like to thank Saint-Gobain Ceramics & Plastics Inc., for donating the TiO_2 powder used in the project.

REFERENCES

[1] S. Michaels, E.M. Sachs, M.J. Cima, Metal parts generation by three dimensional printing, International Solid Freeform Fabrication Symposium. (1992) 244-250.

[2] P.K. Gokuldoss, S. Kolla, J. Eckert, Additive Manufacturing Processes: Selective Laser Melting, Electron Beam Melting and Binder Jetting—Selection Guidelines, Materials. 10 (2017).

[3] R.M. German, Sintering: From Empirical Observations to Scientific Principles, Elsevier Science & Technology Books. (2014).

[4] A.S. Helle, K.E. Easterling, M.F. Ashby, Hot-isostatic pressing diagrams: New developments, Acta Metallurgica. 33 (1985) 2163–2174.

[5] N.B. Crane, J. Wilkes, E. Sachs, S.M. Allen, Improving accuracy of powder sintering-based SFF processes by metal deposition from nanoparticle dispersion, International Solid Freeform Fabrication Symposium. (2005) 261–272.

[6] K. Sato, Y. Hotta, T. Nagaoka, K. Watari, M. Asai, S. Kawasaki, Mutual Linkage of Particles in a Ceramic Green Body through Photoreactive Organic Binders, Journal of the Ceramic Society of Japan. 113 (2005) 687–691.

[7] C.S. Kumar, U.S. Hareesh, A.D. Damodaran, K.G.K. Warrier, Monohydroxy aluminium oxide (Boehmite, AlOOH) as a reactive binder for extrusion of alumina ceramics, Journal of the European Ceramic Society. 17 (1997) 1167–1172.

[8] F.F. Lange, Powder Processing Science and Technology for Increased Reliability, Journal of the American Ceramic Society. 72 (1989) 3-15.

[9] E.M. Sachs, C. Hadjiloucas, S. Allen, H. Yoo, Metal and ceramic containing parts produced from powder using binders derived from salt. (2000). https://patentimages.storage.googleapis.com/b1/f7/47/6e111d964f4fdf/US6508980.pdf.

[10] Y. Bai, C.B. Williams, Binder jetting additive manufacturing with a particle-free metal ink as a binder precursor, Materials & Design. 147 (2018) 146–156.

[11] M.A. Torres Arango, A.S. Valença de Andrade, D.T. Cipollone, L.O. Grant, D. Korakakis, K.A. Sierros, Robotic Deposition of TiO_2 Films on Flexible Substrates from Hybrid Inks: Investigation of Synthesis–Processing–Microstructure–Photocatalytic Relationships, ACS Applied Materials & Interfaces. 8 (2016) 24659–24670.

[12] M.A. Torres Arango, D. Kwakye-Ackah, S. Agarwal, R.K. Gupta, K.A. Sierros, Environmentally Friendly Engineering and Three-Dimensional Printing of TiO_2 Hierarchical Mesoporous Cellular Architectures, ACS Sustainable Chemistry & Engineering. 5 (2017) 10421–10429.

[13] H. Möckel, M. Giersig, F. Willig, Formation of uniform size anatase nanocrystals from bis (ammonium lactato) titanium dihydroxide by thermohydrolysis, Journal of Materials Chemistry. 9 (1999) 3051–3056.

[14] S. Baskaran, L. Song, J. Liu, Y.L. Chen, G.L. Graff, Titanium oxide thin films on organic interfaces through biomimetic processing, Journal of the American Ceramic Society. 81 (1998) 401–408.

[15] Y. Oh, S.-N. Lee, H.-K. Kim, J. Kim, UV-assisted chemical sintering of inkjet-printed TiO_2 photoelectrodes for low-temperature flexible dye-sensitized solar cells, Journal of The Electrochemical Society. 159 (2012) H777–H781.

[16] R. Lupitskyy, V.K. Vendra, J. Jasinski, D.A. Amos, M.K. Sunkara, T. Druffel, Toward high-efficiency dye-sensitized solar cells with a photoanode fabricated via a simple water-based formulation: Toward simple high-efficiency dye sensitized solar cells, Progress in Photovoltaics: Research and Applications. 23 (2015) 883–891.